Fluorescence Emission of Ethidium Bromide Intercalated in Defined DNA Duplexes: Evaluation of Hydrodynamics Components†

Jean Duhamel,‡ Jean Kanyo,§ Gail Dinter-Gottlieb,||,⊥ and Ponzy Lu*,§

Department of Chemistry, University of Waterloo, Waterloo, Ontario N2L 3G1, Canada, Department of Chemistry, University of Pennsylvania, Philadelphia, Pennsylvania 19104, and Department of Bioscience and Biotechnology, Drexel University, Philadelphia, Pennsylvania 19104

Received May 7, 1996; Revised Manuscript Received August 20, 1996⊗

ABSTRACT: The arrangement and stacking of noncovalently contiguous double-helical sections are increasingly invoked in single-stranded DNA and RNA tertiary structure. These tertiary structures of nucleic acids are defined by their double stranded regions, and their orientation in the molecular frame constitutes an important component of the nucleic acid structure. A direct view of these tertiary structures can be obtained by fluorescence polarization anisotropy of bound ethidium bromide (EB). The orientation of the dye in the molecular frame of the nucleic acid yields the orientation of the helix. The complete anisotropy function for EB intercalated in genome-derived DNA duplexes was derived by Allison and Schurr (1979) and accounts for base-pair twisting and DNA bending. Single-stranded ribozymes, ribosomal and transfer RNAs, and model DNA junctions contain double-stranded regions shorter than 35 bp in length, for which bending is not significant. We developed and experimentally verified an expression of the anisotropy function for short DNA duplexes which is theoretically compatible with the existing theory, originally developed for long nucleic acids (Schurr et al., 1992). Simulations showed that for DNA duplexes shorter than 35 bp, our expression of the anisotropy function is equivalent to Schurr's and is consistent with experiments carried out on eight DNA duplexes. Modeling the eight duplexes as cylinders, we calculate a duplex diameter of 1.91 ± 0.15 nm when EB makes a 90° angle with the DNA helix axis and undergoes anisotropic wobbling and 1.97 ± 0.15 nm when EB makes a 70.5° angle and undergoes isotropic wobbling, respectively. We used this treatment to establish the conformation of five DNA oligonucleotides made of single and tethered hairpins, some designed to exhibit coaxial stacking. Analysis of the fluorescence anisotropy decays shows that the tethered hairpins take an extended rather than parallel conformation. It also shows that the DNA oligonucleotides made of two tethered hairpins exhibit freedom compatible with two independent hairpins. When the linker between hairpins is shortened, the two hairpins are not independent anymore as probed by fluorescence anisotropy, suggesting coaxial stacking of the two helices.

We note that the functional forms of single-stranded nucleic acids are defined tertiary structures of loops connecting short double-helical branches and stems. Fluorescence polarization anisotropy (FPA)[1] of a dye bound to a double-helical nucleic acid segment can yield the orientation of the helix in the molecular frame. This is an important piece of structural information. Theory has been developed for describing the anisotropy function of dyes bound to long genome-derived DNA duplexes when collective long-range base-pair twisting and bending are present [Schurr et al. (1992) and references therein; Barkley & Zimm, 1979). It involves a set of four irreducible parameters. They are the persistence length P, the hydrodynamic radius R_H, the torsion constant between base pairs α, and the knowledge of an empirical cutoff frequency k_{max}. P and α are determined by analyzing the early times of the anisotropy decay of a dye bound to large DNA duplexes. The complete anisotropy function is a sum of the products of an exponential series.

For short double-stranded regions, bending for the helices can be neglected. Combining the works by Szabo (1984) and Wahl (1975), we derived an expression for the anisotropy function where bending is ignored and base-pair twisting and bound EB wobbling occur through a diffusional process between two reflecting barriers. Under our experimental conditions (short DNA duplexes less than 35 bp and known dye orientation), an anisotropy decay is described by a sum of three exponentials with two irreducible parameters, the angle l for the delocalization of the dye induced by twisting and wobbling and the hydrodynamic radius of the duplex

† P.L. and G.D.-G. acknowledge research grants from the National Aeronautics and Space Administration and the National Institute of Health, respectively. J.K. was supported in part by National Institutes of Health training grants to the University of Pennsylvania. These experiments were done in part on equipment of the Regional Laser and Biotechnology Laboratories supported by National Institute of Health Research Resource funding to R. M. Hochstrasser.

* To whom correspondence should be addressed.
‡ University of Waterloo.
§ University of Pennsylvania.
|| Drexel University.
⊥ Present address: Department of Biology, Buffalo State College, Buffalo, NY.

⊗ Abstract published in *Advance ACS Abstracts,* December 1, 1996.

[1] Abbreviations: bp, base pair; N_{bp}, number of base pairs; EB, ethidium bromide; FPA, fluorescence polarization anisotropy; $I_{||}(t)$, fluorescence emitted with a polarization parallel to the polarization of the excitation light; $I_{\perp}(t)$, fluorescence emitted with a polarization perpendicular to the polarization of the excitation light; $I(t)$, fluorescence emitted with a polarization at 54.7° (the magic angle) to the polarization of the excitation light; $r(t)$, fluorescence anisotropy; r_0, fluorescence anisotropy at time $t = 0$; τ, lifetime; η, viscosity; T, temperature; l, angle characterizing the delocalization of ethidium bromide after the torsional deformations have decayed away.

S0006-2960(96)01091-4 CCC: $12.00

Table 1: DNA Duplexes Used in This Study

5'-GGATCC CCTAGG-5'	6-mer
5'-AATTGTGAGCG TTAACACTCGC-5'	11-mer
5'-TTGTGAGCGCTCACAA AACACTCGCGAGTGTT-3'	16-mer
5'-TTGTGAGCGGATAACAA AACACTCGCCTATTGTT-5'	17-mer
5'-ACTCTATCATTGATAGAGT TGAGATAGTAACTATCTCA-5'	19-mer
5'-GGACTTCGGTCCTTTTGGACTTCGGTCC CCTGAAGCCAGGAAAACCTCAAGCCAGG-5'	28-mer
5'-GTGGAATTGTGAGCGGATAACAATTTCAC CACCTTAACACTCGCCTATTGTTAAAGTG-5'	29-mer
5'-TTCCGGCTCGTATGTTGTGTGGAATTGTGAGC AAGGCCGAGCATACAACACACCTTAACACTCG-5'	32-mer

R_H. Our treatment of the anisotropy function recovers the diffusion coefficients $D_{||}$ (for diffusion around the helix axis) and $D_\perp$ (for diffusion about the axis perpendicular to the helix axis) independently. With this feature, one can assess whether internal motion is present and whether parallel or perpendicular diffusional motion is affected by it. Finally, the fluorescence anisotropy function is now a sum of three exponentials which can be easily handled by commercially available convolution software packages.

Since our expression of the anisotropy function is based on simplifying assumptions (no bending; base-pair twisting is not a collective process but a diffusional one occurring between two reflecting barriers), it is necessary to assess its limitations. We validated the approach theoretically, by comparing it with the exact solution of Allison and Schurr (1979), and experimentally, through the study of the fluorescence anisotropy of EB intercalated in eight DNA duplexes ranging from 6 to 32 bp (Table 1). We modeled the DNA duplexes as cylinders with rotational motions characterized by diffusional coefficients $D_{||}$ (for the rotation about the helix axis) and $D_\perp$ (for the rotation about the axis perpendicular to the helix axis). In addition to overall tumbling, helix bending, and base-pair twisting, delocalization due to bound EB wobbling needs be considered. Wobbling delocalizes EB orientation in its binding site with motion relative to the nucleic acid on a time scale ($\tau_{osci} <$ 150 ps) (Magde et al., 1983) that is much shorter than the rotational time of an oligonucleotide ($\tau_{rotation}$ [6-mer duplex] = 2 ns). Two cases were considered for wobbling. In case 1, EB was assumed to be perpendicular to the helix axis and to undergo anisotropic wobbling about the helix axis as an extra contribution from base-pair twisting. In case 2, EB's plane was assumed to make an angle θ with the helix axis and to undergo isotropic wobbling. Isotropic wobbling was taken into account by lowering the initial anisotropy from 0.4 to 0.37 (Magde et al., 1983). The angle θ was taken to equal 70.5° (Schurr et al., 1992). Assuming a 0.34-nm rise/base pair, a duplex length increase of 0.27 nm upon intercalation of one EB molecule (Fujimoto et al., 1994), and modeling $D_\perp$ and $D_{||}$ with the Tirado−Garcia de la Torre theory (Tirado & Garcia de la Torre, 1980), analysis of the fluorescence anisotropy with our equation yields a hydrodynamic duplex diameter of 1.91 ± 0.15 nm and for case 1 1.97 ± 0.15 nm case 2. These values are in good agreement with the literature values of 1.99 ± 0.02 nm (Nuuerto et al., 1994) and 2.0 ± 0.15 nm (Eimer et al., 1990).

Single-stranded nucleic acids' tertiary structure is defined, in part, by the spatial orientation of disjointed double-stranded helices. We expanded our approach to handle DNA molecules made of tethered hairpins, either diffusing independently of one another about a common axis or coaxially stacked, a common feature of single-stranded structures. Our simplified equation also describes tethered hairpins if the two hairpins can rotate freely about a common axis. It yields a higher $D_{||}$ value due to enhanced in-plane delocalization stemming from the helices when applied to tethered hairpins, designed to adopt different double-stranded conformations. An equation describing the restricted delocalization of two tethered hairpins rotating about a common axis between two reflecting boundaries is also derived.

EXPERIMENTAL PROCEDURES

Molecular Hydrodynamics. As established by light scattering (Eimer & Pecora, 1991), NMR (Eimer et al., 1990), and transient electric birefringence (Elias & Eden, 1981), the motion of DNA duplexes in solution is best modeled by cylinders. The motion of a cylinder in solution is fully described by the diffusion coefficient about the cylinder symmetry axis $D_{||}$ and about an axis perpendicular to the cylinder symmetry axis $D_\perp$ (Tirado & Garcia de la Torre, 1980; Fujimoto et al., 1994). Tirado and Garcia de la Torre derived the expressions of $D_\perp$ (about an axis perpendicular to the symmetry axis of the cylinder) and $D_{||}$ (about the symmetry axis of the cylinder)

$$D_\perp = \frac{3k_BT}{\pi\eta L^3}(\ln(p) + \delta_\perp) \quad (1)$$

$$D_{||} = \frac{k_BT}{A_0\pi\eta L^3}\left(\frac{4p^2}{1+\delta_{||}}\right) \quad (2)$$

where $p = L/d$, $A_0 = 3.814$, $\delta_{||} = (1.119 \times 10^{-4} + 0.6884/p - 0.2019/p^2)$, and $\delta_\perp = (-0.662 + 0.917/p - 0.05/p^2)$. L is the length of the cylinder, d is the diameter, $\delta_\perp$ is an end-effect correction, and A_0 in eq 2 has been obtained by shell-model calculations. $\delta_{||}$ and $\delta_\perp$ were obtained through interpolations from computer simulations. Equations 1 and 2 are valid for p values between 2 and 30 ($D_{||}$).

We note that the factor of 4 in eq 2 was missing in the original expression of $D_{||}$, eq 74 of Garcia de la Torre and Bloomfield (1981).

Simulation of Vertically and Horizontally Polarized Fluorescence Decays. Vertically and horizontally polarized fluorescence decays were simulated for various DNA duplex lengths, using eq 3, which is the complete expression of the fluorescence anisotropy function for EB bound to long double-stranded DNA with wobbling, twisting, and bending. It was derived by Allison and Schurr (1979). Their expression for the fluorescence anisotropy function is

$$r(t) = r_0 \sum_{n=0}^{2} I_n C_n(t) F_n(t) \quad (3)$$

The initial anisotropy r_0 reflects the local rotational motion of the dye molecule and occurs here in an isotropic manner. The I_n are geometric factors: $I_0 = 0.25(3\cos^2\theta - 1)^2$, $I_1 =$

$3 \sin^2\theta \cos^2\theta$, and $I_2 = 0.75 \sin^4\theta$. The twisting correlation functions $C_n(t)$ were given by

$$C_n(t) = (N+1)^{-1} \sum_{m=1}^{N+1} \exp[-n^2 \sum_{l=2}^{N+1} d_l^2 Q_{ml}^2 [1 - \exp(-t/\tau_1)]] \exp(-n^2 D_{\|} t) \quad (4)$$

where the parameters τ_l, d^2_l, Q_{ml}, and γ are as follows:

$$\tau_l = \frac{\gamma}{4\alpha \sin^2[(l-1)\pi/[2(N+1)]]}$$

$$d_l^2 = \frac{k_B T}{4\alpha \sin^2[(l-1)\pi/[2(N+1)]]}$$

$$Q_{ml} = [2/(N+1)]^{1/2} \cos[(m - {}^1/_2)(l-1)\pi/(N+1)]$$

$$\gamma = \frac{k_B T}{D_{\|}(N+1)}.$$

The tumbling correlation functions $F_n(t)$ are

$$F_n(t) = \exp[-(6-n^2)D_{\perp} t - (6-n^2)A_n \sum_{k=l}^{k_{max}} [1 - \exp(-t/T_k)]/(2k+1)^2] \quad (5)$$

where the parameters A_n, T_k, $D_n(\infty)$, κ_k, and Z_n are as follows:

$$A_n = -\ln[D_n(\infty)]/\exp[(6-n^2)\sum_{k=l}^{k_{max}} 1/(2k+1)^2]$$

$$1/T_k = \frac{k_B T P \kappa_k^4}{4\pi\eta}\left[K_0(\kappa_k R_H) + \left(\frac{\kappa_k R_H}{2}\right) K_1(\kappa_k R_H)\right]$$

$$D_n(\infty) = Z_n^{-1/2} \exp(-Z_n/3)(\pi^{1/2}/2)\mathrm{erf}(Z_n^{1/2})$$

$$\kappa_k = \frac{(2k+1)\pi}{2L} \qquad Z_n = (6-n^2)L/4P$$

R_H is the hydrodynamic radius of the duplex, $D_{\|}$ and $D_{\perp}$ are given in eqs 1 and 2, and L is the length of the duplex.

The decays were convoluted with an experimentally recorded instrument response. Poisson noise was added to the decays (Duhamel et al., 1993). Fluorescence decays were generated assuming absence of free EB and using the following parameters: $r_0 = 0.37$, $P = 1500$ Å, $R_H = 10.7$ Å, $L = N_{bp}(3.4$ Å$) + 2.7$ Å, $T = 293$ K, $\eta = 1.002$ cP, $k_{max} = 10$, $\alpha = 5.4 \times 10^{-12}$ dyne·cm. A lifetime of 23 ns was chosen for EB bound to DNA. The vertically polarized fluorescence decays had 40 000 counts at the maximum and the *G*-factor was taken to equal 1.

Fluorescence Anisotropy Functions. Equation 6 is our simplified anisotropy function of EB bound to a B-DNA helix where (i) DNA bending is negligible for short DNA duplexes, (ii) delocalization of the dye by base-pair twisting and eventually EB wobbling for case 1 occurs through rotational diffusion of EB about the helix axis between two reflecting barriers, making an angle l, and (iii) wobbling and base-pair twisting are internal motions that occur independently of the overall motion.

$$r(t) = r_0\left[0.25\, e^{-6D_{\perp}t}(3\cos^2\theta - 1)^2 + 3\, e^{-(5D_{\perp}+D_{\|})t} \sin^2\theta \cos^2\theta \frac{\sin^2(l/2)}{(l/2)^2} + 0.75\, e^{-(2D_{\perp}+4D_{\|})t} \sin^4\theta \frac{\sin^2 l}{l^2}\right] \quad (6)$$

θ is the angle between the dipole moment μ of EB and the axis Z_P around which delocalization occurs. The dipole moments of absorption μ_A and emission μ_E of EB are equal ($\mu_A = \mu_E = \mu$). In the case of our B-DNA duplexes, $Z_P = Z_M$ where Z_M is the duplex axis. Figure 1 depicts the transition dipoles of the dye in the molecular frame.

Equations 7 and 8 are the anisotropy functions of EB bound to a DNA molecule made of two tethered helices where the assumptions (i−iii) are still valid, (iv) the helices are shorter than 40 bp and EB delocalization due to base-pair twisting and wobbling occurs on a very fast time scale, and (v) the two helices have a coaxial geometry and can rotate independently from one another either freely or in a restricted fashion around their helical axis Z_D fixed in the molecular frame M with $Z_D = Z_M$.

$$r(t) = r_0\left[0.25\, e^{-6D_{\perp}t}(3\cos^2\theta - 1)^2 + 3e^{-[5D_{\perp}+D_{\|}^w]t} \sin^2\theta \cos^2\theta \frac{\sin^2(l/2)}{(l/2)^2} + 0.75e^{-[2D_{\perp}+4D_{\|}^w]t} \sin^4\theta \frac{\sin^2 l}{l^2}\right] \quad (7)$$

In eq 7, $D_{\|}^w = D_{\|} + D$, where D is the rotational diffusion coefficient characterizing the rotation of the helices about Z_M, the helical axis.

$$r(t) = r_0\left[0.25\, e^{-6D_{\perp}t}(3\cos^2\theta - 1)^2 + 3e^{-[5D_{\perp}+D_{\|}]t} \sin^2\theta \cos^2\theta \frac{\sin^2(l/2)}{(l/2)^2}\left(\frac{\sin^2(h/2)}{(h/2)^2} + \frac{1}{(h/2)^2}\sum_{p=1}^{\infty} \exp[-\omega^2(p)Dt]\frac{1-(-1)^p\cos h}{1-\omega^2(p)}\right) + 0.75e^{-[2D_{\perp}+4D_{\|}]t} \sin^4\theta \frac{\sin^2 l}{l^2}\left(\frac{\sin^2 h}{h^2} + \frac{1}{h^2}\sum_{p=1}^{\infty} \exp[-\omega^2(p)Dt]\frac{1-(-1)^p\cos 2h}{[1-\omega^2(p)/4]^2}\right)\right] \quad (8)$$

In eq 8, h is the angle between the two reflecting barriers that restrict the helix delocalization. These equations have been derived in Appendices 1−3.

Materials and Methods. Ethidium bromide (2,7-diamino-10-ethyl-9-phenylphenanthridinium bromide) was obtained from Sigma and was used without further purification. DNA molecules were synthesized using a Milligen Expedite

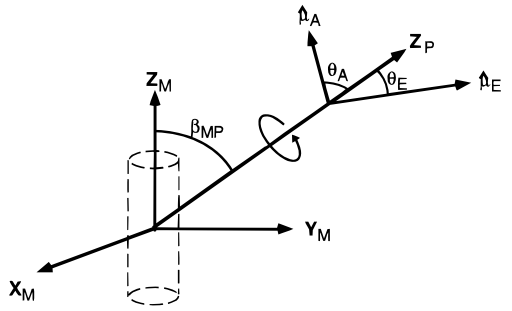

FIGURE 1: Orientations of the transition dipoles of a probe in a cylindrical macromolecule which can internally move about an axis (Z_P) fixed in the macromolecular frame M.

Table 2: DNA Hairpins Used in This Study

DNA0	DNA1A	DNA1B	DNA2	DNA3
T T T T C-G C-G T-A G-C G-C C-G T-A T-A C-G A-T G-C G-C 5'	T C T G C-G C-G G-C G-C 5' T T T T G-C G-C C-G C-G G T C T	T T T T C-G C-G T-A G-C G+T C+T T+C T+G C-G A-T G-C G-C 5'	T C T G C-G A-T G-C G-C 5' T T T T C-G C-G T-A G-C G T C T	TTC T G C-G C-G G-C G-C 5' T T G-C G-C C-G C-G T G TTC	T C T G G-C C-G C-G G-C G-C 5' | G-C G-C C-G C-G G-C T G T C

nucleic acid synthesizer and standard phosphoramidite methodology. They were purified by reverse-phase HPLC. Their sequences are listed in Table 1. To form duplexes, two equal molar amounts of complementary DNA strands were mixed. The solutions were heated up to 95 °C and then slowly cooled overnight to ensure that they would adopt their most thermodynamically stable conformation and to avoid hairpin formation for self-complementary strands. The DNA duplexes were run on a native gel to ensure that no single-stranded material was present. The DNA hairpins DNA0, DNA1, DNA2, and DNA3 (Table 2) were snap-cooled to avoid intermolecular interaction. All experiments were carried out in two buffers (L buffer was 10 mM sodium phosphate and 0.01 mM EDTA, pH = 6.5; D buffer was 100 mM sodium citrate and 50 mM Tris-HCl, pH = 8.5). The viscosities of the solutions were measured on a Brookfield rheometer [for L buffer, η(4 °C) = 1.67 cp and η(22 °C) = 0.93 cp; for D buffer, η(4 °C) = 1.92 cp and η(22 °C) = 1.06 cp].

Absorption and Steady-State Fluorescence Measurements. Absorption measurements were performed on a Beckman spectrophotometer, Model DU 640. Steady-state fluorescence measurements were carried out on a Perkin-Elmer fluorescence spectrophotometer, Model MPF-4.

Binding Constant and Emission of Free EB. In order to estimate the amount of free EB in solution, we calculated the binding constant of EB to our DNA duplexes. Scatchard plots obtained from a combination of absorption and steady-state fluorescence measurements yielded the number of sites, n, available to EB in the DNA molecule and the binding constant K of EB to the DNA molecule. These measurements performed using the 17-mer duplex in L buffer yielded $n = 6$ and $K = 4 \times 10^5$ mol L^{-1}. The fluorescence decay experiments were performed using the same EB concentration of 5×10^{-6} M for all samples. With this EB concentration and a 17-mer duplex concentration of 2.9×10^{-5} M in L-buffer (equivalent to a DNA base pair concentration of 5×10^{-4} M), 1.5% of the EB is free. We performed all our fluorescence decay measurements with a DNA concentration of, at least, 5×10^{-4} M in base pair. We thus ensured a minimum ratio of 200 bases/EB.

Energy Transfer between Two EB Molecules. Energy transfer occurring between two EB molecules located on the same DNA molecule was avoided by adjusting the DNA concentration in order to minimize the number of DNA duplexes having more than one EB. EB was assumed to distribute among the DNA duplexes with a Poisson distribution. Thus, the emission coming from duplexes having more than one EB amounts for ($1\text{-}e^{-N}$) of the total emission, where N is the average occupancy of EB per duplex. With an average occupancy ([EB]/[DNA duplex]) between 0.08 and 0.16 (3.1×10^{-5} M < [DNA duplex] < 6.3×10^{-5} M), the emission arising from DNA duplexes having more than one EB is lower than 15% of the total emission.

Time-Resolved Fluorescence Measurements. Fluorescence decay curves were obtained by a time-correlated single-photon-counting apparatus. Pulsed excitation is obtained from a cavity-dumped dye laser, synchronously pumped by a Nd·YAG laser (Coherent Antares 76-s). The repetition rate of the dye laser was 4 MHz. The samples were contained in a quartz cuvette housed in a thermostated sample holder that was maintained at the desired temperature (4 and 22 °C) within ±1 °C. DNA-bound ethidium bromide was excited with vertically polarized laser pulses at $\lambda_{ex} = 560$ nm, and the emission was detected at 90° to the excitation through a monochromator set at $\lambda_{em} = 610$ nm. At 560 nm, the extinction coefficient is about 5 times in favor of EB bound to DNA rather than free EB in buffer, thus shifting the absorption efficiency toward bound EB and ensuring that less than 1% of the exciting light was absorbed by free EB. The fluorescence decays of EB bound to DNA were obtained by setting the emission polarizer at the magic angle (54.7° with the polarization orientation of the excitation beam). A total of 20 000 counts were stored at the fluorescence decay maximum. Two time-dependent fluorescence intensity decay curves were collected through a polarizing filter which was mechanically rotated so that the filter was oriented alternatively parallel, for $I_{||}(t)$, and perpendicular, for $I_{\perp}(t)$, to the polarization of the excitation beam. At least 15 000 counts were collected at the maximum of $I_{||}(t)$ and 8000 counts at the maximum of $I_{\perp}(t)$. To minimize the effects due to system fluctuation, the orientation of the polarization filter relative to the excitation pulse was changed every 8 s during signal acquisition by a stepping motor, and the polarized fluorescence decay curves were accumulated into two memory addresses in an IBM PC. All fluorescence decays were collected over 450 channels using a time per channel of 173 ps/channel, or 69 ps/channel when more information was needed at the early times. Pulse width at half-maximum is 100 ps.

Data Analysis. Fluorescence decays taken at the magic angle $I(t)$ were first fitted with a biexponential where the short lifetime was fixed to that of free EB ($\tau = 1.7$ ns). The recovered long lifetime was around 23 ns, characteristic of intercalated EB (Lakowicz, 1983), and good χ^2 were obtained ($\chi^2 < 1.2$). In order to ensure a best fit, the decays were then fitted with a triexponential function (eq 9a). One lifetime was fixed to the lifetime of free EB (1.7 ns). The two longer lifetimes were attributed to EB bound to DNA. Fluorescence decays polarized parallel [$I_{||}(t)$] and perpendicular [$I_{\perp}(t)$] to the polarization of the excitation light were

analyzed simultaneously by convoluting the instrument response function with eq 9b for $I_{||}(t)$ and eq 9c for $I_{\perp}(t)$.

$$I(t) = a_F e^{-t/\tau_F} + a_{B1} e^{-t/\tau_{B1}} + a_{B2} e^{-t/\tau_{B2}} \quad (9a)$$

$$I_{||}(t) = a_F e^{-t/\tau_F} + (a_{B1} e^{-t/\tau_{B1}} + a_{B2} e^{-t/\tau_{B2}})[1 + 2\, r(t)] \quad (9b)$$

$$I_{\perp}(t) = a_F e^{-t/\tau_F} + (a_{B1} e^{-t/\tau_{B1}} + a_{B2} e^{-t/\tau_{B2}})[1 - r(t)] \quad (9c)$$

The parameters a_F, τ_F, a_{B1}, τ_{B1}, a_{B2}, and τ_{B2} are fixed in the analysis of the polarized decays. The *G*-factor was calculated from the initial amplitudes of the vertically and horizontally polarized fluorescence decays of free EB. The anisotropy function was either a single-, double-, or triple-exponential function and its parameters were forced to remain the same in the simultaneous analysis of the two decays. For the decays collected either at magic angle or at a given polarization angle, the parameters were retrieved by using a least-squares curve-fitting program based on the Marquardt−Levenberg algorithm (Press et al., 1992). The χ^2 values retrieved for the analysis of the polarized decays are calculated over both fluorescence decays and reflect the best fit going through both decays. The fitting procedure was started two or three channels after the instrument function maximum. For small l angles ($l < 50°$), the $(\sin^2 l)/l^2$ terms were approximated using the first two terms of the Taylor series. Fitting the fluorescence decays yields the two rotational times τ_1 [$= (2D_{\perp} + 4D_{||})^{-1}$] and τ_2 [$= (6D_{\perp})^{-1}$] and the angle l.

RESULTS

EB binds to DNA duplexes by intercalation (Tsai et al., 1977, Meyer-Almes & Porschke, 1993) between two DNA base pairs (a binding constant of 4×10^5 mol L^{-1} was calculated in the case of the 17-mer duplex in L buffer). Upon binding of EB to DNA, the absorption spectrum is shifted to the red, the fluorescence spectrum is shifted to the blue and the lifetime of EB lengthens from 1.7 ns in buffer (as measured with our SPC spectrometer) to about 23 ns when bound to DNA.

In order to ensure a best fit, our decays were fitted with eq 9a, a sum of three exponentials. The fits were slightly improved ($\chi^2 < 1.1$) compared to that obtained with two exponentials ($\chi^2 < 1.2$). The recovered parameters were used in the analysis of the fluorescence anisotropy decays. Since the preexponential weight of the third exponential was smaller than 20%, little physical meaning was attributed to this extra exponential. However, it has already been reported that EB intercalated in DNA duplexes exhibits a slightly biexponential decay (Hernandez et al., 1994). The shorter lifetime was assumed to originate from EB molecules bound in the vicinity of the fraying ends of the duplex. In our decays, the contribution from free EB was never larger than 5% of the total fluorescence intensity. A triexponential fit of magic-angle fluorescence decay of EB bound to a 29-bp DNA duplex is presented in Figure 2.

An example of the light intensities collected with a polarization orientation parallel, $I_{||}(t)$, and perpendicular, $I_{\perp}(t)$, to the polarization of the excitation beam is shown in Figure 3. At early times, $I_{||}(t)$ experiences a fast decay characteristic of the transport of vertically polarized molecules to the horizontal plane of polarization, whereas $I_{\perp}(t)$ exhibits a rise-time that characterizes the build up of a population of horizontally polarized molecules. At longer times, both $I_{||}(t)$ and $I_{\perp}(t)$ traces decay parallel with the fluorescence decay trace taken at magic angle. In this time regime, all molecules have averaged their orientations and decay by natural fluorescence.

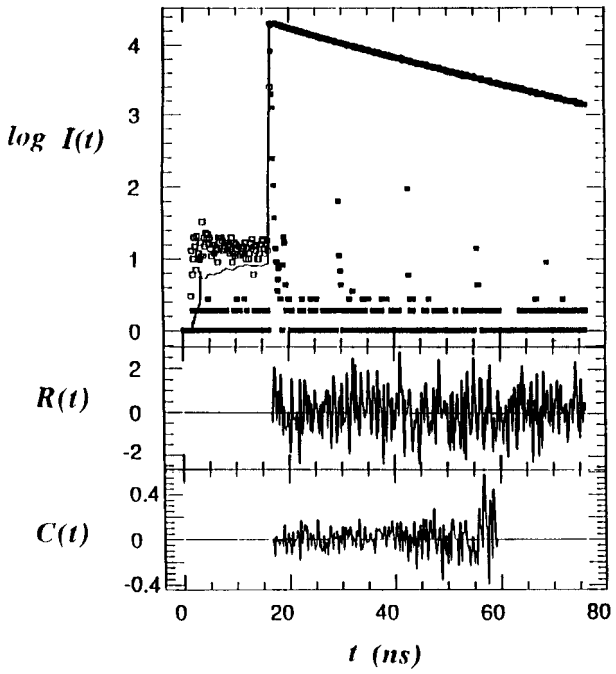

FIGURE 2: Fluorescence decay curve of EB bound to the 29-bp DNA duplex in D buffer collected at magic angle and fitted with eq 9a. $\lambda_{ex} = 560$ nm and $\lambda_{em} = 610$ nm. $R(t)$ is the residual of the fit and $C(t)$ is the autocorrelation function of the residuals.

As a first approximation, the fluorescence decays were fitted assuming that the DNA duplexes were spheres of equivalent hydrodynamic volume V_H. In this case $D_{||}$ and $D_{\perp}$ are supposed to be equal and the anisotropy function expressed in eq 6 becomes monoexponential:

$$r(t) = r_0 \exp[-t/\tau_{sph}] \quad (10)$$

where r_0 is the initial anisotropy which characterizes the extent of EB delocalization. The fitting of the fluorescence decays yielded values for r_0, τ_{sph}, and χ^2 that are listed in Tables 3 and 4. As expected, we observe that, with increasing duplex length, the χ^2 values become larger, consistent with the geometry of DNA duplexes which differs more and more from a sphere with increasing length.

A linear increase of $\tau_{sph}T/\eta$ vs N_{bp} is obtained as shown in Figure 4, confirming that a hydrodynamic treatment of the data is correct. From the slope of this straight line, we estimate the average volume occupied by one base pair to be 1.7 nm^3. For a cylinder with a height of 0.34 nm, this is a diameter of 2.5 nm, within the limits of the DNA duplex diameters obtained experimentally (Tirado et al., 1984).

We refined our analysis by using eq 6 for the anisotropy function, assuming 70.5° and 90° for the EB angle θ to the helix axis. Assigning the values of the angle θ defining the position of EB in the molecular frame of a B-DNA helix turns out to be a delicate matter. On the one hand, X-ray crystal structures of EB intercalated in a miniduplex made of two dinucleoside monophosphates show that the plane of EB is parallel to the plane of the base pair (Tsai et al., 1977). Thus, the Euler angle θ characterizing the angle between

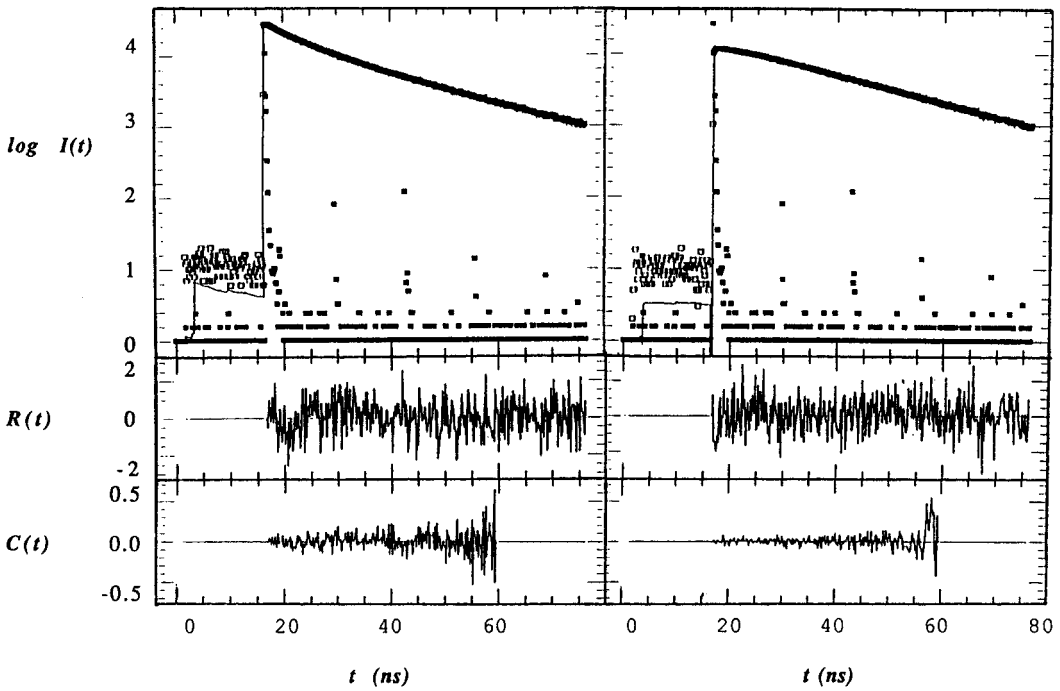

FIGURE 3: Fluorescence decay curves of EB bound to the 29-bp DNA duplex in D buffer collected through a polarization filter oriented parallel $I_{\parallel}(t)$ and perpendicular $I_{\perp}(t)$ to the polarization of the exciting beam. $r(t)$ was fitted with two exponentials according to eq 6 with $\theta = 90°$. $\lambda_{ex} = 560$ nm and $\lambda_{em} = 610$ nm.

Table 3: Emission Anisotropy Decay Parameters for Ethidium Bromide Bound to DNA in L and D Buffer at 22 °C[a]

molecule	buffer	r_0	τ_{rot} (ns)	χ^2
6-mer	L buffer	0.33	1.9	1.51
	D buffer	0.32	2.1	1.21
11-mer	L buffer	0.35	3.5	1.13
	D buffer	0.32	4.0	1.27
16-mer	L buffer	0.33	5.2	1.50
	D buffer	0.34	5.7	1.89
17-mer	L buffer	0.33	6.5	1.47
	D buffer	0.33	8.1	1.74
19-mer	L buffer	0.31	7.0	1.53
	D buffer	0.33	7.9	1.39
29-mer	L buffer	0.31	11.4	1.73
	D buffer	0.31	12.3	1.87
32-mer	L buffer	0.31	14.4	1.97
	D buffer	0.31	15.3	2.44

[a] The anisotropy function is a single exponential.

Table 4: Emission Anisotropy Decay Parameters for Ethidium Bromide Bound to DNA in L and D Buffer at 4 °C[a]

molecule	buffer	r_0	τ_{rot} (ns)	χ^2
11-mer	L buffer	0.31	6.9	1.22
	D buffer	0.34	7.8	1.70
17-mer	L buffer	0.33	12.1	2.60
	D buffer	0.33	13.8	2.18
19-mer	L buffer	0.29	13.2	1.56
	D buffer	0.30	15.9	1.86
29-mer	L buffer	0.29	21.0	1.64
	D buffer	0.29	24.2	2.05
32-mer	L buffer	0.32	24.0	3.19
	D buffer	0.30	27.9	2.20

[a] The anisotropy function is a single exponential.

μ_A or μ_E and the DNA helix axis can be approximated to 90°. On the other hand, reduced linear dichroism data carried out on long DNA duplexes show that, upon intercalation in B-DNA helices, θ equals 70.5° (Hogan et al., 1979). Although these last results have been questioned (Charney et al., 1986), the condition $\theta = 70.5°$ has been used successfully to fit fluorescence decays of EB bound to DNA

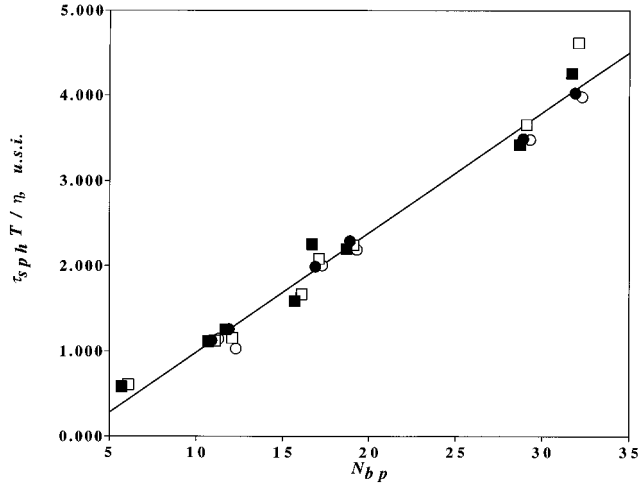

FIGURE 4: Plot of $\tau_{sph}T/\eta$ vs N_{bp}. Experimental data: (□) duplexes in L buffer at 22 °C; (○) duplexes in L buffer at 4 °C; (■) duplexes in D buffer at 22 °C; (●) duplexes in D buffer at 4 °C. To avoid overlap, the abscissa was slightly offset in order to spread the data points.

(Schurr et al., 1992). Thus, we decided to consider both options for analyzing our fluorescence decays assuming anisotropic wobbling about the helix axis with $\theta = 90°$ (case 1) and isotropic wobbling with $\theta = 70.5°$ (case 2).

From the analysis of the fluorescence decays with eq 6, we retrieved the two rotational times τ_1 and τ_2 and the delocalization angle l, which values are listed in Tables 5 and 6 for $\theta = 90°$ and anisotropic wobbling. The χ^2 are much improved over the whole range of duplex lengths, but they did not exhibit differences that would justify considering case 1 rather than case 2. Furthermore, they do not exhibit the systematic increase with duplex length that we observed with the spherical approximation ($\tau_{sph} = \eta V/k_BT$), which means that the asymmetry of the DNA duplexes is well accommodated by eq 6. We also observe an increase of the delocalization angle l with duplex length ranging at 22 °C

Table 5: Emission Anisotropy Decay Parameters for Ethidium Bromide Bound to DNA in L and D Buffer at 22 °C[a]

molecule	buffer	τ_1 (ns)	τ_2 (ns)	l (deg)	χ^2
11-mer	L buffer	3.1	4.5	38.8	1.10
	D buffer	3.3	5.7	37.7	1.23
16-mer	L buffer	3.9	8.9	43.2	1.29
	D buffer	4.4	9.9	40.7	1.62
17-mer	L buffer	4.5	11.6	39.4	1.16
	D buffer	4.9	18.6	34.9	1.02
19-mer	L buffer	4.6	13.0	45.2	1.13
	D buffer	5.2	15.3	39.1	1.07
28-mer	L buffer	6.8	28.1	43.5	1.82
	D buffer	7.4	30.1	42.7	1.56
29-mer	L buffer	6.5	26.3	42.4	1.06
	D buffer	7.3	28.4	44.5	0.96
32-mer	L buffer	8.3	35.2	43.7	1.07
	D buffer	8.6	38.7	44.2	1.25

[a] The anisotropy function is a biexponential according to eq 6 with $\theta = 90°$.

Table 6: Emission Anisotropy Decay Parameters for Ethidium Bromide Bound to DNA in L and D Buffer at 4 °C[a]

molecule	buffer	τ_1 (ns)	τ_2 (ns)	l (deg)	χ^2
11-mer	L buffer	5.2	10.8	50.6	1.17
	D buffer	6.1	12.3	41.0	1.49
17-mer	L buffer	8.2	24.1	39.6	1.69
	D buffer	9.3	28.0	41.8	1.49
19-mer	L buffer	8.1	26.8	53.6	1.02
	D buffer	9.7	34.2	51.1	1.13
29-mer	L buffer	12.3	50.1	53.2	1.08
	D buffer	13.1	70.2	53.3	1.08
32-mer	L buffer	15.1	75.0	48.4	1.41
	D buffer	15.7	86.5	51.7	1.19

[a] The anisotropy function is a bi-exponential according to eq 6 with $\theta = 90°$.

from about 38° for the 11-mer duplex up to 44° for the 32-mer duplex for case 1.

DISCUSSION

To derive eq 6, we have assumed that base-pair twisting and eventually EB wobbling delocalize EB by an angle l about the helix axis on a time scale much faster than overall tumbling of the duplex and that DNA bending is negligible for short DNA duplexes. In order to assess the validity limit of eq 6, we have simulated vertically and horizontally polarized decays for cases 1 ($\theta = 90°$ and $r_0 = 0.40$) and 2 ($\theta = 70.5°$ and $r_0 = 0.37$), using the complete form of the fluorescence anisotropy function derived by Schurr and Allison (1979). The parameters employed for the simulations are listed in the Experimental Procedures section. The results obtained from the analysis by eq 6 of the decays simulated with eq 3 assuming either cases 1 or 2 yielded the same τ_1, τ_2, and l values for DNA duplexes shorter than 40 bp. We report here the results obtained with case 2.

For each DNA duplex length, vertically and horizontally polarized fluorescence decays were generated to which five different Poisson noise sequences were added (Duhamel et al., 1993). The resulting fluorescence decays were analyzed using eq 6. The fits were perfect, with χ^2 between 0.90 and 1.05, and showed randomly distributed residuals and autocorrelation function of the residuals. The values τ_1, τ_2, and l obtained for one DNA duplex length and the corresponding set of five fluorescence decays were averaged and plotted in Figure 5. DNA duplexes with 10, 20, 30, 40, 50, 60, and 70 bp were used to simulate fluorescence decays. We monitored the rotational lifetimes τ_1 and τ_2:

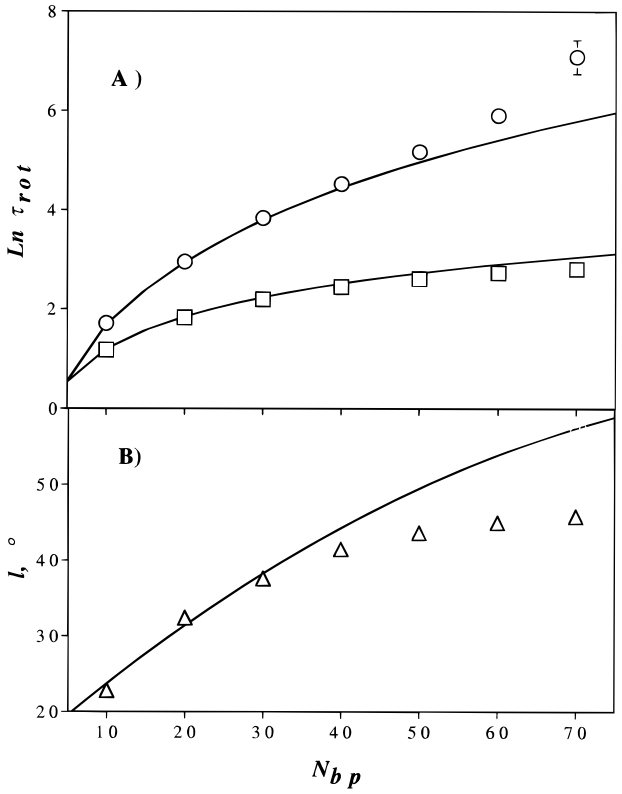

FIGURE 5: (A) Plot of ln τ_1 (□) and ln τ_2 (○) vs N_{bp}. The errors are smaller than the symbols. The solid lines indicate the theoretical rotational times. (B) Plot of l vs N_{bp}. The solid line represents the l value obtained by comparing the residual amplitudes of $C_n(t)$ in eqs 3 and A5 after the torsional deformations have decayed away.

$$\tau_1 = (4D_{\parallel} + 2D_{\perp})^{-1} \quad (11a)$$

$$\tau_2 = (6D_{\perp})^{-1} \quad (11b)$$

where $D_{\parallel}$ and $D_{\perp}$ are given in eqs 1 and 2.

Figure 5A represents the theoretical and fitted lifetimes τ_1 and τ_2 versus DNA duplex length. The calculated errors are smaller than the symbols in the figure. For long DNA duplexes (>70 bp), our analysis software could not retrieve τ_2 because of the slow tumbling of these long DNA duplexes. For a DNA duplex of 70 bp, τ_2 calculated under our simulation conditions is equal to 403 ns, which is 17-fold larger than the natural lifetime of EB (23 ns) and thus recovered with little accuracy. Figure 5B shows the delocalization angle l due to base-pair twisting. It increases with DNA duplex length. We also compared the l values retrieved with eq 6 with those obtained from the residual amplitude of $C_n(t)$ in eq 3 after the torsional deformations have decayed away (Nuuerto et al., 1994; their eq 12). Figure 5 shows that for duplexes having less than 40 bp, the difference between the τ_1, τ_2, and l values expected theoretically [eq 3] and retrieved with eq 6 is smaller than 5%.

For DNA duplex lengths smaller than 40 bp, we have established that our eq 6 is in good agreement with eq 3 which more completely describes the delocalization of EB through wobbling, base-pair twisting, DNA bending, and overall tumbling. Thus, we can now proceed with the hydrodynamic analysis of our rotational times obtained with eq 6.

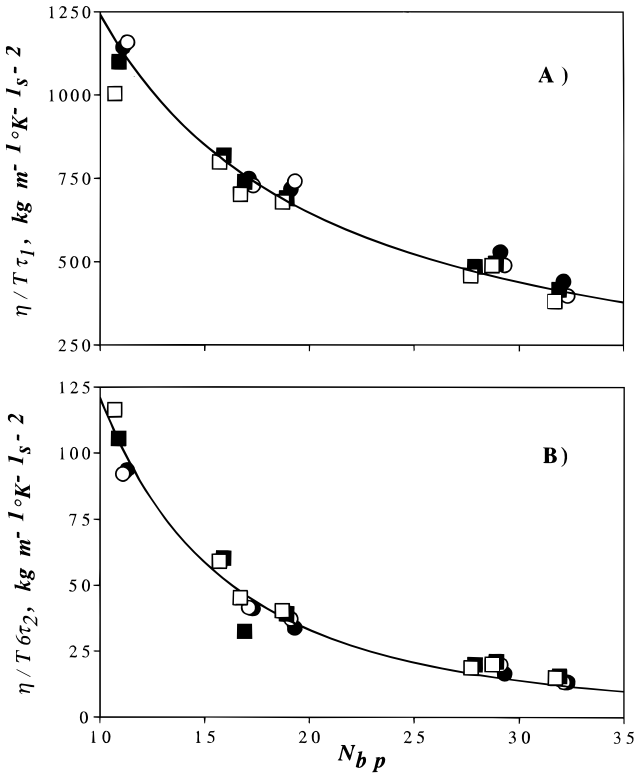

FIGURE 6: (A) Plot of $\eta/T\tau_1$ vs N_{bp}. Experimental data: (□) duplexes in L buffer at 22 °C; (○) duplexes in L buffer at 4 °C; (■) duplexes in D buffer at 22 °C; (○) duplexes in D buffer at 4 °C. The best fit is shown for $d = 1.91$ nm. To avoid overlap, the abscissa was slightly offset in order to spread the data points. (B) Plot of $\eta/T6\tau_2$ vs N_{bp}. Experimental data: (□) duplexes in L buffer at 22 °C; (○) duplexes in L buffer at 4 °C; (■) duplexes in D buffer at 22 °C; (●) duplexes in D buffer at 4 °C. The best fit is shown for $d = 1.91$ nm. To avoid overlap, the abscissa was slightly offset in order to spread the data points.

Equations 1 and 2 give the expressions of the rotational diffusion coefficients for the lengthwise ($D_{||}$) and the sidewise ($D_{\perp}$) motions, respectively. Assuming that the duplex length increases by 0.34 nm/base pair and that addition of one EB lengthens the duplex length by 0.27 nm (Nuuerto et al., 1994), we were able to compute the cylinder diameter by fitting the whole set of τ_1 and τ_2 values with eq 11. The fit of the data obtained with an angle θ equal to 90° is shown in Figure 6. Assuming case 1 and case 2, we obtained a cylinder hydrodynamic diameter of 1.91 ± 0.15 and 1.97 ± 0.15 nm, respectively. These values are in good agreement with previous studies [Eimer & Pecora, 1991 (2.0 ± 0.15 nm); Tirado et al., 1984 (2.0 nm < diameter < 2.8 nm); Nuuerto et al., 1994 (1.99 ± 0.02 nm)].

Taking a duplex diameter of 1.91 nm and assuming a duplex length equal to (N_{bp}0.34 + 0.27) nm, we can calculate τ_1 and τ_2 from eqs 1, 2, and 11a for DNA duplexes 10−35 bp in length. The power law given in eq 12 fits the data well

$$\frac{\eta}{T\tau_i} = A_i N_{bp}^{B_i} \qquad (12)$$

where the index i is either 1 or 2. The A_i and B_i parameters are listed in Table 7. Equation 12 can also be rearranged to yield an expression relating τ_1 to τ_2:

$$\tau_1 = \frac{\eta}{TA_1}\left(\frac{TA_2}{\eta}\right)^{B_1/B_2} \tau_2^{\,B_1/B_2} \qquad (13)$$

Table 7: Result of the Fit of the Ratios $\eta/T\tau_i$ by Equation 12

i	A_i	B_i
1	11 620	−0.95
2	86 680	−2.04

When calculating the hydrodynamic parameters τ_1 and τ_2 of an oligonucleotide, this set of equations gives insight whether an oligonucleotide behaves as a rigid B-DNA duplex or whether extra internal motion is present.

Application to Coaxial Stacking. In multibranched DNA/RNA molecules, coaxial stacking of helices is assumed to be energetically favorable. Coaxial stacking has been directly observed by NMR in an immobile DNA junction (Pikkermaat et al., 1994) and by X-ray crystallography as a feature of the three-dimensional shape of t-RNA (Kim et al., 1974). It is present in group I introns (Murphy et al., 1994). Pseudoknots are hypothesized to be stabilized by coaxial stacking (Dam et al., 1992). We can measure the diffusional coefficient about the helix axis $D_{||}$ to answer questions relevant to coaxial stacking. Our strategy is simple. $D_{||}$ depends on the geometry of the tethered helices. As a result, if a DNA/RNA molecule is made of two unstacked helices, they should exhibit quite different $D_{||}$ coefficients from that of two coaxially stacked helices.

We designed five 28-base-long DNA molecules with increasing propensity to undergo coaxial helical stacking. Their sequences are shown in Table 2. They are made of one or two hairpins which end with a 5′-TTCG tetraloop, except for DNA2, which is made of two hairpins with 4 bp stems capped with the pentaloops 5′-TTTCG and 5′-GCTTT. DNA0 is a fully complementary hairpin (HP) with a 12-base-pair stem. DNA1A is made of two hairpins with 4-base-pair stems, tethered by four thymines. DNA1B can take two conformations. One possibility is the same as for DNA1A; the other is a hairpin with a 12-base-pair stem having four mismatches in the double helix, indicated by + signs in Table 2. A 12-base-pair RNA duplex analog to the hypothetical 12-base-pair stem of DNA1B has been observed to take this conformation in a crystal lattice (Holbrook et al., 1991). DNA3 is made of two hairpins with a 5-base-pair stem, directly connected without a linker. DNA3 has a high probability of undergoing coaxial stacking.

For each DNA molecule, the fluorescence decays $I_{||}(t)$, $I_{\perp}(t)$, and $I(t)$ were measured. We assumed that due to electrostatic repulsion DNA1A, DNA1B, DNA2, and DNA3 would take an elongated conformation, similar in shape to a 13/15-base-pair duplex. DNA0 is a control that is supposed to behave like a 13/15-base-pair duplex as well. Consequently, we used eq 6 as the expression for the anisotropy function. The following discussion deals with the results obtained by fitting the fluorescence decays of EB bound to the hairpins with eq 6 assuming an angle θ equal to 90°. These data are shown in Table 8. The same conclusions were reached by assuming an angle θ equal to 70.5°, but the data are not listed. Using eq 12 for the experimentally obtained τ_2 value, we assess the associated number of base pairs for the molecule considered. Using eq 13, we calculate from the experimentally obtained τ_2 value the expected τ_1 value, were the oligonucleotide a perfect duplex. The data obtained with this approach yield striking conclusions. The expected τ_1 values are listed in Table 8.

For all five molecules, N_{bp} retrieved from the analysis of τ_2 yields values between 13.0 and 15.8. These values are

Table 8: Emission Anisotropy Decay Parameters for Ethidium Bromide Bound to the DNA Hairpins in L and D Buffer at 22 °C[a]

molecule	buffer	τ_1 (ns)	τ_2 (ns)	l (deg)	χ^2	expected τ_1 (ns)	N_{bp}
DNA0	L	3.4	7.2	43.5	1.43	3.2	13.4
	D	4.1	8.5	37.8	1.50	3.7	13.6
DNA1A	L	2.0	6.9	38.8	1.21	3.1	13.2
	D	2.5	7.7	38.3	1.07	3.5	13.0
DNA1B	L	2.2	6.9	35.5	1.18	3.1	13.2
	D	2.6	7.8	40.9	1.37	3.6	13.0
DNA2	L	2.5	8.7	38.2	1.50	3.5	14.8
	D	3.2	10.4	38.7	1.68	4.1	15.0
DNA3	L	3.9	10.0	38.0	1.50	3.7	15.8
	D	4.3	11.6	38.4	1.67	4.3	15.8

[a] The anisotropy function is a biexponential According to eq 6 with $\theta = 90°$. Expected τ_1 is obtained by introducing τ_2 into eq 13. N_{bp} is obtained from the τ_2 values and eq 12.

reasonable for an extended conformation of these DNA molecules, which validates our assumption and allows us to apply eq 7 or 8 for the anisotropy function in case of enhanced delocalization due to independent helix rotation. The experimentally observed τ_1 values for DNA1A, DNA1B, and DNA2 listed in Table 8 are about 40% smaller than expected, implying additional delocalization in the base-pair plane. We attribute this effect to internal rotation of the helices as described by eq 7. Only for DNA0 and DNA3 do the expected τ_1 values match the experimentally observed ones. We take this as an indication that the two helices forming DNA3 are coaxially stacked.

Conclusion. We have developed simple expressions of the fluorescence anisotropy of EB intercalated in short DNA duplexes and in tethered hairpins. Assuming that EB intercalation occurs in the plane parallel to the base pairs and perpendicular to the helix axis, a duplex diameter of 1.91 nm was obtained. We applied these results for assessing the conformation of tethered DNA hairpins with stems having different extents of double-stranded regions. We showed that these hairpins adopt extended rather than folded conformations and were able to probe coaxial stacking. Assuming free rotation of the tethered DNA hairpins about the molecular axis, the associated rotational diffusion coefficient was calculated. These equations take EB wobbling and base-pair twisting into account and allow us to derive structural information. We anticipate that this approach coupled with site-specific insertion of fluorescent dyes will be useful to describe functional single-stranded RNA/DNA structures.

APPENDIX 1: ANISOTROPY FUNCTION OF EB BOUND TO A B-DNA HELIX

The following assumptions were made: (i) DNA bending is negligible for short DNA duplexes. (ii) Delocalization of the dye by base-pair twisting and eventually EB wobbling for case 1 occurs through rotational diffusion of EB about the helix axis between two reflecting barriers. (iii) Wobbling and base-pair twisting are internal motions that occur independently of the overall motion.

Our derivation is based on the works of Szabo (1984) and Wahl (1975). With our assumptions, we can apply the expression derived by Szabo (1984; his eq 4.6) for the anisotropy function of a probe moving in a restricted fashion about an axis Z_P fixed in the molecular frame (X_M, Y_M, Z_M) of a symmetric-top macromolecule:

$$r(t) = \frac{2}{5}\sum_{amn} e^{-[6D_\perp + a^2(D_\parallel - D_\perp)t]} d^{(2)}_{an}(\beta_{MP}) d^{(2)}_{am}(\beta_{MP}) \times \Gamma_{nm}(t) \cos(m\alpha_E - n\alpha_A) d^{(2)}_{m0}(\theta_E) d^{(2)}_{n0}(\theta_A) \quad \text{(A1)}$$

where β_{MP}, θ_A, and θ_E are defined in Figure 1 and α_A and α_E are the dihedral angles between the Z_M vector and μ_A and μ_E, respectively. μ_A and μ_E are the absorption and emission dipoles, respectively. In the case of EB, μ_A and μ_E are parallel so that the quantities indexed by A and E are equal and the index has been dropped in the following equations. The rotation matrices are derived by Wigner (1959). $\Gamma_{nm}(t)$ is the azimuthal correlation function and is given by

$$\Gamma_{nm}(t) = \langle e^{-in\gamma_{MP}(t)} e^{im\gamma_{MP}(0)} \rangle \quad \text{(A2)}$$

where $\Omega_{MP} = (\alpha_{MP}, \beta_{MP}, \gamma_{MP})$ are the Euler angles which transform the M frame of the macromolecule into the P frame of the probe.

In our case, the angle γ_{MP} is diffusing between two reflecting barriers, one for $\gamma_{MP} = 0$ and the other for $\gamma_{MP} = l$. From Wahl (1975, his eqs 8, 41, and 43), we derive the expression of the azimuthal correlation function:

$$\Gamma_{nm}(t) = \frac{4}{mn\, l^2} e^{-i(l/2)(m-n)} \sin\left(m\frac{l}{2}\right) \sin\left(n\frac{l}{2}\right) - \frac{2}{l^2}\sum_{p=1}^{\infty} mn \frac{[1-(-1)^p e^{-iml}][(-1)^p e^{+inl} - 1]}{[n^2 - \omega^2(p)][m^2 - \omega^2(p)]} \exp\left(\frac{p^2\pi^2 Dt}{l^2}\right) \quad \text{(A3)}$$

with $\omega(p) = p\pi/l$ and D is the rotational diffusion coefficient for the motion of EB about the axis Z_P. In the case of EB rotating about the B-DNA helix, the axes Z_M and Z_P are parallel and β_{MP} is equal to zero. The Wigner rotation matrix $d^{(2)}_{\mu\lambda}$ ($\beta_{MP} = 0$) is the unity matrix so that only the diagonal terms remain in eq A1, implying $a = m = n$. The complete form of the anisotropy function is

$$r(t) = 0.1\, e^{-6D_\perp t}(3\cos^2\theta - 1)^2 + 1.2\, e^{-(5D_\perp + D_\parallel)t} \sin^2\theta \cos^2\theta \left[\frac{\sin^2(l/2)}{(l/2)^2} + \frac{1}{(l/2)^2}\sum_{p=1}^{\infty} \exp(-\omega^2(p)Dt) \frac{1-(-1)^p \cos l}{[1-\omega^2(p)]^2}\right] + 0.3\, e^{-(2D_\perp + 4D_\parallel)t} \sin^4\theta \left[\frac{\sin^2 l}{l^2} + \frac{1}{l^2}\sum_{p=1}^{\infty} \exp[-\omega^2(p)Dt] \frac{1-(-1)^p \cos 2l}{[1-\omega^2(p)/4]^2}\right] \quad \text{(A4)}$$

For long cylinders ($D_\perp = D_\parallel = 0$), eq A4 reduces to the expression derived by Wahl (1975) for immobile cylinders. Actually, eq A4 can easily be put into the form of eq 3 if

we take the following expressions for r_0, I_n, $F_n(t)$, and $C_n(t)$ ($n = 0, 1, 2$). We call this new form of eq 3 eq A5.

$$r(t) = r_0 \sum_{n=0}^{2} I_n C_n(t) F_n(t) \tag{A5}$$

where $r_0 = 0.4$ for case 1 or $r_0 = 0.37$ for case 2, $I_0 = 0.25\text{-}(3\cos^2\theta - 1)^2$, $I_1 = 3\sin^2\theta\cos^2\theta$, $I_2 = 0.75\sin^4\theta$, $F_n(t) = 1.0$ (we assumed no bending), $C_0(t) = 1.0$, and

$$C_1(t) = \frac{\sin^2(l/2)}{(l/2)^2} + \frac{1}{(l/2)^2}\sum_{p=1}^{\infty} \exp[-\omega^2(p)Dt]\,\frac{1-(-1)^p\cos l}{[1-\omega^2(p)]^2}$$

$$C_2(t) = \frac{\sin^2(l)}{l^2} + \frac{1}{l^2}\sum_{p=1}^{\infty} \exp[-\omega^2(p)Dt]\,\frac{1-(-1)^p\cos 2l}{[1-\omega^2(p)/4]^2}$$

For short duplexes, one can assume that delocalization motions occur on a fast time scale [$\omega^2(p)D \gg 2D_\perp + 4D_\parallel$ for all values of p] and the anisotropy function tends to the expression

$$r(t) = r_0\left[0.25\,e^{-6D_\perp t}(3\cos^2\theta - 1)^2 + 3\,e^{-(5D_\perp + D_\parallel)t}\sin^2\theta\cos^2\theta\,\frac{\sin^2(l/2)}{(l/2)^2} + 0.75\,e^{-(2D_\perp + 4D_\parallel)t}\sin^4\theta\,\frac{\sin^2 l}{l^2}\right] \tag{A6}$$

Equation A6 is eq 6 in the main text. Equation A6 is a sum of three exponentials where the lifetimes yield the two diffusion coefficients of the object and the angle l yields the extent of delocalization due to twisting and eventually wobbling for case 1. For no delocalization ($l = 0$), eq A6 reduces to the classic anisotropy function derived for symmetric-top molecules (Chuang & Eisenthal, 1972). Assuming EB perpendicular to the helix axis ($\theta = \pi/2$) and anisotropic wobbling about the helix axis (case 1), eq A6 further simplifies and yields

$$r(t) = 0.1\,e^{-6D_\perp t} + 0.3\,\frac{\sin^2 l}{l^2}\,e^{-(2D_\perp + 4D_\parallel)t} \tag{A7}$$

APPENDIX 2: ANISOTROPY FUNCTION OF EB BOUND TO A DNA MOLECULE MADE OF TWO TETHERED HELICES

To the three assumptions (i−iii) of Appendix 1, we added the following ones: (iv) The helices are short ($N_{bp} < 40$) and EB delocalization due to base-pair twisting and wobbling occurs on a very fast time scale. (v) The two helices have a coaxial geometry and can rotate independently from one another either freely or in a restricted fashion around their helical axis Z_D fixed in the molecular frame M with $Z_D = Z_M$. The anisotropy function is given by the following equation (Wittebort & Szabo, 1978):

$$r(t) = \frac{2}{5}\sum_{amnpq} e^{-[6D_\perp + a^2(D_\parallel - D_\perp)]t}\langle D^{(2)}_{an}[\Omega_{MD}(t)]D^{(2)}_{am}{}^*[\Omega_{MD}(0)]\rangle \times \langle D^{(2)}_{np}[\Omega_{DP}(t)]D^{(2)}_{mq}{}^*[\Omega_{DP}(0)]\rangle\langle D^{(2)}_{p0}[\Omega_{PF}(t)]D^{(2)}_{q0}{}^*[\Omega_{PF}(0)]\rangle \tag{A8}$$

where $D^{(2)}_{an}$ is a Wigner rotation matrix element, Ω_{MD} is the Euler angle that transforms the molecular frame M into the helix frame D with $Z_M = Z_D$, Ω_{DP} is the Euler angle that transforms the helix frame D into the frame P attached to the probe with $Z_D = Z_P$, and $\Omega_{PF}(0)$ and $\Omega_{PF}(t)$ are the Euler angles which give in the P frame the orientation of the absorption and emission dipolar moments, respectively. $D_\perp$ and $D_\parallel$ are the rotational diffusion coefficients of the whole object, i.e., the macromolecule made of two tethered DNA helices. Using Appendix 3, the fluorescence anisotropy function can be rewritten as

$$r(t) = \frac{2}{5}\sum_{a} e^{-[6D_\perp + a^2(D_\parallel - D_\perp)]t}\langle e^{-ia\gamma_{MD}(t)}e^{-ia\gamma_{MD}(0)}\rangle \times \langle e^{-ia\gamma_{DP}(t)}e^{-ia\gamma_{DP}(0)}\rangle \times \cos[a(\alpha_E - \alpha_A)]d^{(2)}_{a0}(\theta_E)d^{(2)}_{a0}(\theta_A) \tag{A9}$$

where the angles α_A, α_E, θ_A and θ_E have been defined in Appendix 1. The expression of the two azimuthal functions in eq A9 is given in eq A3 for rotation about an axis between two reflecting barriers.

In the case of free rotation of the helices about Z_M, the azimuthal correlation function was derived by Wahl (1975):

$$\langle e^{-ia\gamma_{MD}(t)}e^{-ia\gamma_{MD}(0)}\rangle = e^{-a^2Dt} \tag{A10}$$

where D is the rotational diffusion coefficient characterizing the rotation of the helices about Z_M. Taking into consideration assumption (iv) and since EB has parallel absorption and emission dipolar moments, the expression of the anisotropy function for free rotation about Z_M is

$$r(t) = r_0\left[0.25\,e^{-6D_\perp t}(3\cos^2\theta - 1)^2 + 3\,e^{-[5D_\perp + D_\parallel{}^w]t}\sin^2\theta\cos^2\theta\,\frac{\sin^2(l/2)}{(l/2)^2} + 0.75\,e^{-[2D_\perp + 4D_\parallel{}^w]t}\sin^4\theta\,\frac{\sin^2 l}{l^2}\right] \tag{A11}$$

where $D_\parallel{}^w = D_\parallel + D$ and $r_0 = 0.4$ when EB wobbling occurs in the base-pair plane and $r_0 = 0.37$ when EB wobbling occurs in an isotropic fashion. It appears that, in the case of free rotation of the helices about Z_M, the anisotropy function takes an expression equivalent to eq A6. However, $D_\parallel{}^w$ takes a larger value due to enhanced delocalization from helix rotation. Equation A11 is eq 7 in the main text.

When the helices undergo delocalization about Z_M within an angle h, the following expression for the fluorescence

anisotropy is obtained using the derivation of the azimuthal function given in Appendix 3:

$$r(t) = r_0\Bigg[0.25\, e^{-6D_\perp t}(3\cos^2\theta - 1)^2 + 3e^{-[5D_\perp + D_\parallel]t}\sin^2\theta\cos^2\theta\,\frac{\sin^2(l/2)}{(l/2)^2}\Bigg(\frac{\sin^2(h/2)}{(h/2)^2} + \frac{1}{(h/2)^2}\sum_{p=1}^{\infty}\exp[-\omega^2(p)Dt]\frac{1-(-1)^p\cos h}{1-\omega^2(p)}\Bigg) + 0.75\, e^{-[2D_\perp + 4D_\parallel]t}\sin^4\theta\,\frac{\sin^2 l}{l^2}\Bigg(\frac{\sin^2 h}{h^2} + \frac{1}{h^2}\sum_{p=1}^{\infty}\exp[-\omega^2(p)Dt]\frac{1-(-1)^p\cos 2h}{[1-\omega^2(p)/4]^2}\Bigg)\Bigg] \quad \text{(A12)}$$

Equation A12 is eq 8 in the main text. A similar derivation using eq 4.31a−c of Schurr et al. (1992) can be made by taking $\epsilon_0 = \mu_0$, $\zeta_0 = 0$, and $\omega = 0$.

APPENDIX 3

A Wigner rotation matrix element $D^{(2)}_{ab}(\Omega_{IJ})$ can be expressed as follows:

$$D^{(2)}_{ab}(\Omega_{IJ}) = D^{(2)}_{ab}(\alpha_{IJ}, \beta_{IJ}, \gamma_{IJ}) = e^{-ia\alpha_{IJ}}d^{(2)}_{ab}(\beta_{IJ})e^{-ib\gamma_{IJ}}$$

where the reduced matrix elements $d^{(2)}_{ab}(\beta_{IJ})$ are real and satisfy the orthonormality condition. In the case where the frame J can only rotate about Z_I and $Z_I = Z_J$, then $\alpha_{IJ}(t) = \alpha_{IJ}(0)$ and $\beta_{IJ}(t) = \beta_{IJ}(0) = 0$ and the correlation function reduces to the azimuthal function:

$$\langle D^{(2)}_{an}[\Omega_{IJ}(t)]D^{(2)*}_{am}[\Omega_{IJ}(0)]\rangle = \langle e^{-ia\alpha_{IJ}(t)}d^{(2)}_{an}[\beta_{IJ}(t)] \times e^{-in\gamma_{IJ}(t)}e^{+ia\alpha_{IJ}(0)}d^{(2)}_{am}[\beta_{IJ}(0)]e^{+im\gamma_{IJ}(0)}\rangle = \langle e^{-ia\gamma_{IJ}(t)}e^{+ia\gamma_{IJ}(0)}\rangle$$

which is independent of n and m ($a = n = m$).

REFERENCES

Barkley, M. D., & Zimm, B. H. (1979) *J. Chem. Phys. 70*, 2991−3007.

Charney, E., Chen, H. H., Henry, E. R., & Rau, D. C. (1986) *Biopolymers 25*, 885−904.

Chuang, T. J., & Eisenthal, K. B. (1972) *J. Chem. Phys. 57*, 5094−5097.

Dam, E. T., Pleij, K., & Draper, D. (1992) *Biochemistry 31*, 11665−11676.

Duhamel, J., Yekta, A., Ni, S., Khaykin, Y., & Winnik, M. A. (1993) *Macromolecules 26*, 6255−6260.

Eimer, W., & Pecora, R. (1991) *J. Chem. Phys. 94*, 2324−2329.

Eimer, W., Williamson, J. R., Boxer, S. G., & Pecora, R. (1990) *Biochemistry 29*, 799−811.

Elias, J. G., & Eden, D. (1981) *Macromolecules 14*, 410−419.

Fujimoto, B. S., Miller, J. M., Ribeiro, N. S., & Schurr, J. M. (1994) *Biophys. J. 67*, 304−308.

Garcia de la Torre, J., & Bloomfield, V. A. (1981) *Q. Rev. Biophys. 14*, 81−139.

Hernandez, L. I., Zhong, M., Courtney, S. H., Marky, L. A., & Kallenbach, N. R. (1994) *Biochemistry 33*, 13140−13146.

Hogan, M., Dattagupta, N., & Crothers, D. M. (1979) *Biochemistry 18*, 280−288.

Holbrook, S. R., Cheong, C., Tinoco, I., Jr., & Kim, S.-H. (1991) *Nature 353*, 579−581.

Kim, S.-H., Suddath, F. L., Quigley, G. J., McPherson, A., Sussman, J. L., Wang, A. H. J., Seeman, N. C., & Rich, A. (1974) *Science 185*, 435−440.

Lakowicz, J. R. (1983) *Principles of Fluorescence Spectroscopy*, Chapters 6 and 7, Plenum Press, New York and London.

Magde, D., Zappala, M., Knox, W. H., & Nordlund, T. M. (1983) *J. Phys. Chem. 87*, 3286−3288.

Meyer-Almes, F. J., & Porschke, D. (1993) *Biochemistry 32*, 4246−4253.

Murphy, F. L., Wang, Y.-H., Griffith, J. D., & Cech, T. R. (1994) *Science 265*, 1709−1712.

Nuuerto, S., Fujimoto, B. S., Flynn, P. F., Reid, B. R., Ribeiro, N. S., & Schurr, J.M. (1994) *Biopolymers 34*, 463−480.

Pikkermaat, J. A., Van den Elst, H., van Boom, J. H., & Altoma, C. (1994) *Biochemistry 33*, 14896−14907.

Press, W. H., Flaaery, B. P., Tenkolsky, S. A., & Vetterling, W. T. (1992) *Numerical Receipes in Fortran: The Art of Scientific Computing*, pp 523−528, Cambridge University Press, Cambridge, England, and New York.

Schurr, J. M., Fujimoto, B. S., Wu, P., & Song, L. (1992) in *Topics in Fluorescence Spectroscopy, Volume 3: Biochemical Applications* (Lakowicz, J. R., Ed.) pp 137−229, Plenum Press, New York.

Szabo, A. (1984) *J. Chem. Phys. 81*, 150−167.

Tirado, M. M., & Garcia de la Torre, J. (1980) *J. Chem. Phys. 73*, 1986−1993.

Tirado, M. M., Lopez Martinez, M. C., & Garcia de la Torre, J. (1984) *J. Chem. Phys. 81*, 2047−2052.

Tsai, C.-C., Jain, S. C., & Sobell, H. M. (1977) *J. Mol. Biol. 114*, 301−315.

Wahl, P. (1975) *Chem. Phys. 7*, 210−219.

Wigner, E. P. (1959) *Group Theory and its Application to the Quantum Mechanics of Atomic Spectra*, pp 167 and 212, Academic Press, New York.

Wittebort, R. J., & Szabo, A. (1978) *J. Chem. Phys. 69*, 1722−1736.

BI9610919